INSTITUTE OF AEROPHYSICS

UNIVERSITY OF TORONTO

DEVELOPMENT OF A PROPULSION SYSTEM FOR POWERING A SELF-PROPELLED GETOL MODEL AIRCRAFT

by

R. C. Radford

DECEMBER, 1962

UTIA TECHNICAL NOTE NO. 64

VTH

terugbezorgen voor:	terugbezorgen voor:

N.B. **Uitleentermijn:** boeken, rapporten, e.d.
maximaal 3 maanden
losse tijdschriftnummers maximaal 2 weken

DEVELOPMENT OF A PROPULSION SYSTEM FOR POWERING A SELF-PROPELLED GETOL MODEL AIRCRAFT

by

R. C. Radford

DECEMBER, 1962 UTIA TECHNICAL NOTE NO. 64

ACKNOWLEDGEMENTS

The author wishes to express his gratitude to Dr. G. N. Patterson, the Director of the Institute of Aerophysics, for the opportunity to conduct this research.

Special thanks are extended to Professor B. Etkin for his advice and guidance from conception of the project to the review of the final manuscript.

The author is indebted to G. Kurylowich for his assistance in the experimental work and in the calculations for the fan design.

This work was made possible by the financial support of the Defence Research Board of Canada and the United States Airforce, Aeronautical Systems Division, (Contract AF 33(657)-8451, monitored by the Flight Control Laboratory, Aerospace Mechanics Branch).

SUMMARY

An estimate of the propulsion system requirements for the second UTIA GETOL model was determined from the data and theory contained in the available literature on ground effect phenomena.

A dynamometer was designed and built to determine the torque - speed characteristics of model aircraft engines. Three engines were tested to find one that had the power required.

A ducted-fan and straightener system which would utilize this power output was designed and built. It was installed in a cylindrical duct for testing. The pressure rise, power required and efficiency as functions of volume flow at constant r.p.m. were determined for the fan and straightener combination.

TABLE OF CONTENTS

NOTATION

A_b	wing base area exclusive of peripheral jet slot (square feet)
A_j	peripheral jet exit area (square feet)
A_L	lift augmentation
$\bar{c}$	wing mean chord (feet)
g	gravitational constant
h	height of vehicle above ground
H	head; output of fan, ft. - lb per lb of gas
J	scalar jet momentum flux at peripheral jet (pounds)
K_1	ratio of internal losses to mean peripheral jet dynamic pressure
K_2	ratio of internal losses to fan pressure rise
ΔP	static pressure rise through fan and straighteners (p. s. f.)
P_l	internal duct losses (p. s. f.)
P_T	total pressure of peripheral jet (p. s. f.)
Q	volume flow through fan (c. f. m.)
q_j	mean dynamic pressure of peripheral jet (p. s. f.)
u_2	circumferential velocity of fan blade at its r. m. s. height ft. /sec.
W	gross vehicle weight (lb)

NOTATION - continued

β_1	fan blade inlet angle
β_2	fan blade exit angle
β_3	stator inlet angle
ρ	density of air (slugs per cubic ft.)
ϕ	capacity coefficient; the ratio of the axial velocity of the flow to the circumferential velocity of the fan blade at its r.m.s. height
$\psi = \frac{Hg}{u_2^2}$	head coefficient

I. INTRODUCTION

Initial testing of the first GETOL model aircraft on the UTIA circular track facility indicated that a more efficient model would have to be built (Ref. 1). It was found that removing the base plate and operating the model as a plenum chamber vehicle allowed it to achieve operating heights two to three times those observed in the peripheral jet configuration. This indicated that the pressure drop in the internal ducting and wing interior in the peripheral jet configuration was too great and that the fan was operating at very low efficiency. It was also found that reducing the number of fan blades from 12 to 6 produced a slight improvement in performance.

This was considered sufficient evidence that the engine and fan were improperly matched to the power requirements of the internal ducting of the model.

Thus, it was decided to design and build a ducted fan propulsion system which would be properly matched to the power available from a model aircraft engine.

This project has been concerned with the selection of a suitable model aircraft engine power plant and the design and static testing of the fan-straightener system to be installed in the second GETOL model.

II. APPARATUS

2.1 Engine Dynamometer

Having established the approximate propulsion system power requirements on the basis of an estimated gross vehicle weight and geometry, (see appendix), a dynamometer was constructed to test a series of model aircraft motors in order to find one with the necessary power.

The dynamometer (Fig. 1 and 2) utilizes the deflection of a torsion rod to measure the torque output of the motor under test. The engine is attached co-axially to a stiff shaft which is supported in a pillow block by two ball bearings. The other end of this shaft is connected to a rigid end plate by means of a long hollow torsion rod. Care was taken to ensure that the engine drive shaft, the stiff support rod, and the torque rod were all co-axial. Thus the motor can rotate in the bearings, constrained only by the torque rod. Damping is provided by a paddle wheel immersed in an oil bath mounted between the stiff shaft and the torsion rod. A pointer is attached to the torque rod on the end nearest the motor and deflections are read from a large scale mounted behind the pointer.

The engine can be locked in position for starting, after which it is released and it rotates through an angle proportional to its torque output. The deflection of the support shaft in comparison to that of the torque rod is negligible.

The engine is surrounded with a cylindrical shroud to guide the air over the cylinder head for better cooling. Before each set of tests, the engine and shaft assembly were detached from the torque rod and carefully balanced so that no torques due to gravity would be produced.

Reverse pitch propellors were used to produce the load on the engines. In this way the air was blown away from the engine and apparatus to minimize the possibility of the airstream interacting with its surroundings.

The torque rods were calibrated by replacing the engine and its mount by a pulley of 2.2" diameter. A light chord was fastened to the bottom of the pulley and run over the top of the pulley and down one side. Weights were hung from the free end of the chord and the angular deflection of the rod was read from the scale.

2.2 Fan Test Rig

The outer wall of the test duct (see Fig. 3 and 4) is a cylinder of transparent acrylic plastic with an I.D. of 5" and an O.D. of 5 1/2", separable at the section passing through the fan to allow access to the fan and flow straighteners. The duct is flanged at this section and is held together by three bolts. The front of the cylinder is fitted with a wooden bellmouth inlet of circular section (radius 1"). The exit of the duct can be fitted with orifice plates with hole diameters ranging from 1/2" to 5" dia. (fully open) in 1/2" increments to vary the loading on the fan (see Fig. 5).

The front hub, turned from aluminum, houses one of the three fan drive shaft bearings. Its elliptic section proved effective in keeping the flow attached. Kerosene and lamp black studies showed no separation of the flow up to the fan. The front hub is held in the duct by five tandem pairs of steel rods, around which are fitted five symmetrical airfoil-like shrouds to minimize losses.

The rear hub or diffusion cone, is of a conical section and subtends an angle of about 26° at its rear. Seven stators are attached to the rear hub with seven steel rods passing through their leading edges. These rods serve the dual purpose of supporting the cone and blades and acting as an axle about which these blades can pivot,

Pins imbedded in the blades near their trailing edges pass through circular arc slots in the duct wall and fit into holes in a slip ring

passing around the duct. By rotating the slip ring, the blades can be made to pivot about the front rods. In this way, the stators can be adjusted to compensate for any rotation the flow may have as it leaves the stator trailing edge, thus keeping the flow as close to axial as possible (Fig. 6).

In order that construction be as simple and as fast as possible, the fan and straightener vanes were made from balsa wood by an experienced model builder. The steel peripheral ring on the fan (Fig. 7) adds to its structural integrity and was expected to help minimize tip losses. Unfortunately, due to the method of construction of the fan, rather generous tolerances had to be allowed for, particularly the radial clearance between the fan and duct wall.

The fan drive shaft is connected to a 1 H.P. A/C motor by means of a flat belt and pulley system. The fan drive shaft is supported by three bearings, one on either side of the pulley and the one previously mentioned in the front hub.

The free running speed of the fan shaft with no fan attached is 9840 r.p.m. For r.p.m. measurements a tachometer generator is connected to the front of the fan shaft. The output of the generator is fed to an electronic counter with a variable display time (see Fig. 8).

Static pressure taps are located in the wall of the duct at the inlet and at a position aft of the stators. Four taps are arranged circumferentially around the wall at each station. Three holes are also located at each of these stations to allow static and total head probes to be inserted for the purpose of radially traversing the duct.

2.3 Apparatus for Torque (H.P.)-R.P.M. Calibration of Fan Drive Shaft

In order to measure the power input to the fan, it was necessary to obtain a torque - r.p.m. curve for the fan drive shaft.

For this purpose, the fan was replaced by a flat faced pulley of 2" dia. A frictional force was applied to the pulley by means of a flat leather belt passing around the pulley with its ends attached to a horizontal beam on either side of the beam's pivot point. One end of the beam is supported by a spring balance (see Fig. 9).

The friction force generated at the pulley-belt interface causes a different tension force in the two ends of the belt. This produces a couple about the beam pivot point equal to the torque output of the shaft. The beam is prevented from rotating and is maintained in a horizontal plane by the force in the spring balance. This force measured by the spring balance is proportional to the torque as well. From the geometry of the system the torque output can be calculated from the force measurement. An r.p.m. measurement taken at the same time as the force measurement gives one point of the torque - r.p.m. curve.

The torque and r.p.m. were varied by changing the height of the beam pivot point, thus altering the friction force exerted by the belt on the pulley.

III. EXPERIMENTAL RESULTS

3.1 Calibration of Engine Dynamometer

Two different torque rods were used in the testing of the three model engines. The .19 and .25 cu. in. displacement engines were tested with a 14 gauge stainless steel hypodermic tube torque rod and the .35 engine with a heavier 13 gauge rod. This was done to ensure a strength and sensitivity of the torque rod appropriate to the power output of the engine under test.

Each calibration was repeated several times and the mean slope was obtained for each rod.

The sensitivity of the 14 gauge rod was estimated by theoretical calculation to be .00195 ft-lb/drgree. The mean slope of the calibration curves was .00179 ft-lb/degree.

For the 13 gauge rod, the predicted and measured sensitivities were .0034 and .0030 ft-lb/degree respectively. The discrepancies in measured and predicted sensitivities could be due to errors in the sectional geometry and shear modulus used in the calculations.

The calibration curves for the two torque rods are shown in Figs. 10 and 11.

3.2 Engine Characteristics

Three model aircraft engines were tested. Their displacements were .19, .25 and .35 cu. in. respectively. The fuel used was a standard model engine fuel having a 5% nitromethane content. The .35 cu. in. engine was fitted with a throttle control, which allowed the fuel-air mixture to be varied continuously to produce a wide range of power outputs. For this engine, three H.P. vs. r.p.m. curves were found for three throttle settings.

The method of testing was as follows. The needle valve was adjusted so that the engine ran smoothly at its peak r.p.m. as indicated by a strobotac with the propellor recommended by the manufacturer. The needle valve position was marked and left at this setting for all subsequent tests.

After starting the engine, the locking mechanism was released and the engine allowed to rotate to its equilibrium position. The angular displacement was noted on the scale and the r.p.m. measured with a strobotac pointed at the propellor. This enabled one point on the torque - r.p.m. curve to be computed. The torque and r.p.m. were varied by changing the load on the engine, that is by using propellors of varying diameter and number of blades. Enough points were measured, in each case, to produce a torque - r.p.m. curve covering a range of several thousand r.p.m. on either side of the r.p.m. for maximum H.P.

All engines operated very smoothly and at no time did the pointer oscillate by more than $\pm 2^{o}$ (corresponding to torques of $\pm$.0036 and .0060 ft-lb for the 14 gauge and 13 gauge torque rods respectively). In any case, the mean pointer position was easily estimated. The curves for the three engines are shown in Figs. 12 to 14 inclusive.

As a result of these tests, the .35 engine was selected as a suitable power plant because its power output exceeded the minimum requirements established during preliminary design.

3.3 Torque (H.P.) - R.P.M. Calibration of Fan Drive Shaft

Since the power output of the fan drive shaft is largely dependent on the condition and tension of the belt which transmits the power from the motor to the shaft, the calibration curve was measured before and after the fan testing to ensure that no appreciable changes had taken place.

It was suspected that increasing the normal force on the pulley might increase the frictional losses in the bearing in the front hub. This would have the effect of reducing the apparent power output of the shaft (i.e. decrease the slope of the H.P. vs r.p.m. curve). To determine the magnitude of this effect the belt was oiled and greased to reduce the coefficient of friction between the two surfaces. In this way a greater normal force would have to be applied to the pulley to produce the same torque. It was found that the effect of oiling the belt was negligible.

The results of the calibrations are shown in Fig. 15.

3.4 Fan Characteristics

Static wall tap readings were taken at the fan inlet and stator exit for 9 orifice plate diameters ranging from 5" (fully open) to 1" in 1/2" increments . Wall tap readings were also taken between the fan and stator sections in an attempt to determine the pressure rise in each of the two stages. Because the taps were located very close to the recess in the duct wall, which introduced unknown errors, and because it was found to be impossible to make traverses at this section to correlate with the wall tap readings it was decided to omit these results. The maximum

pressure rise was found to occur for an orifice diameter of 3 1/2". Simultaneous r.p.m. measurements enabled the input power to be calculated for each orifice plate from the H.P. - r.p.m. calibration of the drive shaft.

It was found that for orifice plates of diameters less than 3", some high pressure air was escaping frontwards through the fan. The loss appeared to be occurring between the peripheral ring of the fan and the duct wall. Thus the 3" diameter plate was considered to mark the practical lower limit of volume flow which can be delivered by the fan.

Static pressure traverses were made of the inlet and total pressure traverses at the stator exit position along three radii for the 4 1/2", 3 1/2" and modified 3 1/2" diameter orifice plates. These measurements were graphically integrated with a planimeter to find the true volume flow and pressure rise as a function of the volume flow and pressure rise indicated by the wall taps. These calculations were plotted and used to correct all the wall tap results, assuming that interpolation was valid. The corrections to volume flow were of the order of 2% and to pressure rise of the order of 5%

Typical velocity and pressure distributions as a function of radius are presented in Fig. 16. For a fixed geometry, the fan volume flow varies as the r.p.m. and the pressure rise as the $(r.p.m.)^2$. Using this fact the fan pressure rise and volume flow for each orifice plate were corrected to a common speed. Figure 17 shows the fan-stator pressure rise as a function of volume flow corrected to a speed of 10,000 r.p.m. Also plotted is the overall efficiency and power input.

Wool tufts and kerosene and lamp-black were used for flow visualization to determine the behaviour of the flow at the fan inlet and stator sections of the duct.

IV. DISCUSSION OF RESULTS

If the design pressure rise and volume flow at 12,400 r.p.m. (see Appendix I) are reduced to equivalent values at 10,000 r.p.m. it is found that the design pressure rise and volume flow are 30.4 p.s.f. and 5.27 c.f.s. respectively. Referring to Fig. 17 it is seen that, at the best efficiency point, the fan pressure rise is 14.6 p.s.f. and the volume flow 5.75 c.f.s. Thus while only 48% of the design pressure rise was realized, the design volume flow was exceeded by about 9%

The reduced performance can be partly traced to the low efficiency. Lamp-black and kerosene coated on the stators revealed that even at the best efficiency point, the flow over the upper surface of the stators had separated. Also, due to the method of construction of the fan

rather large clearances had been allowed between the running parts, particularly the radial clearance. Both of these factors could cause the low efficiency observed. However, even if the efficiency were as much as 85%, for the same power input and mass flow, the pressure rise would only be increased by about 4.5 p.s.f. Thus it would appear that this fan is incapable of producing the design pressure rise. The fan inlet angles, β_1, conform very well to the theoretical angles (see Fig. 18 and Appendix I) but due to the fact that the blades were designed with a linear twist, as a concession to ease of construction, the blade exit angles deviate by approximately $+4^o$ at the root to -4^o at the tip from forced vortex angles. It is felt that these deviations, plus any additional errors which were incurred during construction, combined to reduce the output capabilities of the fan.

V. CONCLUSIONS

Although the fan straightener system fails to produce the design pressure rise, it is expected that the fan, when driven by the model aircraft engine, will produce sufficient power that the model performance will be adequate (see Appendix II).

If testing of the completed model reveals that the assumptions regarding losses were optimistic rather than pessimistic then there are several alternatives to obtain increased air power output: (i) a redesign of the fan in order to gain the necessary output, or (ii) increasing the output of the present fan. The latter could be accomplished by lengthening the stator blades to prevent separation of the flow. (iii) The greatest increase in output would be realized with the use of a "hotter" fuel in the engine (that is to say, a fuel with a higher nitroparafin content). Manufacturer's curves show increases in power of the order of 25% or greater with the use of these fuels.

REFERENCES

1. Liiva, J. — A Facility for Dynamic Testing of Models of Airborne Vehicles with Ground Effect. UTIA Tech. Note No. 53, Oct. 1961.

2. Dau, K. — Characteristics of a Rectangular Wing with a Peripheral Jet in Ground Effect, Part I. UTIA Tech. Note No. 56, Sept. 1961.

3. Chaplin, H.R. — Design Study of a 29-foot GEM. DTMB Aero Report 999, April 1961.

4. Stepanoff, A.J. — Turboblowers, John Wiley and Sons, 1955.

5. Chaplin, H.R. — A Preliminary Design Technique for Annular Jet Ground-Effect Machines (GEMS). DTMB Aero Report 966, Sept. 1959.

6. Cohen, H.
Rogers, G.F.C. — Gas Turbine Theory. Longmans Green and Co.

APPENDIX I - DESIGN OF FAN

The pressure rise and volume flow requirements of the fan were established on the basis of an assumed vehicle weight, wing planform, and desired hover height.

The following characteristics were therefore assumed:

planform:	rectangular (rounded edges)
weight:	4 lb.
aspect ratio:	2.85
chord:	7"
desired h/c:	0.1
gap thickness:	0.1"

For the design h/c a lift augmentation A_L of 2.2 was assumed. For a higher aspect ratio wing (A.R. = 4.17), Dau (Ref. 2) measured a value of A_L = 3.15 at this h/c.

The assumed A_L allows for a smaller augmentation than that of the Dau model.

Using simple theory, the total pressure (above atmospheric) of the peripheral jet is given by

$$P_T = \Delta P - P_l \tag{1}$$

The average static pressure in the peripheral jet is assumed to be half the base pressure. Thus the jet dynamic pressure can be related to the fan pressure rise by

$$\Delta P = \frac{P_b}{2} + P_l + q_j \tag{2}$$

Assuming the jet exit angle is zero and neglecting the contribution of static pressure on the peripheral jet exit area Chaplin's equation for augmentation becomes (Ref. 5)

$$A_L = 1 + \frac{P_b A_b}{J} \tag{3}$$

Expressing the internal losses between fan and jet exit as a fraction of the exit dynamic pressure ($P_l = K_1 q_j$)and substituting for the exit dynamic pressure in terms of jet momentum, the following is derived

$$\Delta P = \frac{J}{2}\left[\frac{A_L - 1}{A_b} + \frac{1 + k_1}{A_j}\right] \qquad (4)$$

The jet momentum is $J = W/A_L = 1.82$.

Chaplin (Ref. 3) assumes internal losses to be 50% of inlet dynamic pressure. In this case it is assumed that the internal losses are 75% of exit dynamic pressure (i.e. $k_1 = .75$). Equation 4 then yields a value of $P = 43.6$ p.s.f. From the jet momentum, the volume flow is calculated to be 5.35 c.f.s. For an overall efficiency of 85%, the fan would require an input power of about .5 H.P.

These requirements were taken to be the minimum for the fan.

In order to pass the required volume flow through a fan of reasonable size, the outer diameter of the fan was set at 5". The number of blades was set at 6 to make the construction relatively easy. From the empirical data found in Ref. 4, the fan hub to tip ratio was found to be .5 for 6 blades. After a trial and error process, it was found from the design chart in Ref. 4 that an operating point of $\phi = .3$ and $\psi = .43$ for a blade exit angle of 40° at the r.m.s. radius would produce a satisfactory fan output. For an assumed efficiency of 85% the power required curve of the fan should intersect the power available curve of the engine at a speed of 12,400 r.p.m. and a H.P. of .65. The output of the fan at this speed is $\Delta P = 46.8$ p.s.f. and $Q = 6.53$ c.f.s. (see Fig. 19).

The theoretical fan inlet angles, β_1, were calculated assuming a constant axial velocity across the radius and assuming a zero angle of attack at the entrance. The theoretical exit angles, β_2, were calculated assuming a forced vortex pattern of flow. A graph of the theoretical angles and those actually used in the fan blades is presented in Fig. 18.

Certain concessions to ease of construction were made in the selection of the blade angles actually used in that the blades were to have a constant camber and a linear twist from root to tip. Thus the inlet angles are very close to theoretical design values but the exit angles vary from -4° to $+3.4^\circ$ from forced vortex angles at the root and tip respectively. The blades have a constant circular-arc camber line with a linear twist of 12.3° from root to tip. The blade thickness about the camber line is that of the British C4 profile. The blades have a constant chord of 2.3" in accordance with the empirical rule that the chord/spacing ratio be less than unity.

The theoretical straightener angles, β_3, allow for a certain amount of "slip" as the flow leaves the fan. The theoretical and actual straightener angles are shown in Fig. 18. The length of the straighteners was dictated largely by the requirement of keeping the length of the fan straightener system moderately short so that the nacelle of the final model would not be too long. It may be that had this design restriction not been imposed, and longer-chord straighteners used, the flow might have remained attached over the straighteners and not separated as was actually observed.

APPENDIX II - MODEL HOVER PERFORMANCE ESTIMATE

In order to estimate the hover performance of the second GETOL model with the measured fan performance, the following augmentation values, for a series of $h/\bar{c}$ ratios, were assumed.

$h/\bar{c}$	A_L
.05	4.20
.10	2.20
.15	1.53
.20	1.20

These values would place the assumed augmentation curve midway between the curves of Dau and Poisson-Quinton shown in Ref. 2. It is felt that these are conservative augmentation estimates. In the following analysis it is assumed that the augmentation is independent of gap width.

If the average peripheral jet static pressure is 1/2 the base pressure the following equation relates the fan pressure rise and exit dynamic pressure

$$P_T = \Delta P - P_\ell = \frac{P_b}{2} + q_j \qquad \text{(II. 1)}$$

The internal duct losses are expressed as a fraction of the fan pressure rise ($P_\ell = K_2 \Delta P$).

Thus,

$$\Delta P (1 - K_2) = \frac{P_b}{2} + q_j \qquad \text{(II. 2)}$$

Neglecting the contribution to lift of the static pressure in the jet and assuming a uniform base pressure and a thin vertical peripheral jet the following relation can be written

$$A_L = 1 + \frac{P_b A_b}{J} = \frac{W}{J} \qquad \text{(II. 3)}$$

The model has the following characteristics:

W: 4 lb
A_b: .695 ft^2

Using the above equations and data with the relation

$$q_j = \frac{1}{2} \frac{J^2}{\rho Q^2} \qquad \text{(II. 4)}$$

graphs are plotted in Fig. 20 relating the loss factor K_2 and the jet exit area to the $h/\bar{c}$ ratio, for two sets of values of ΔP and Q, corresponding to fan operation at the best efficiency point and maximum pressure rise point.

On the graphs, the exit areas at which the fan operated at its best efficiency point and maximum pressure rise point in the test rig are shown. If internal losses in the test rig are identical to those in the model an estimation of the $h/\bar{c}$ ratio could be obtained from this. The $h/\bar{c}$ ratios are .09 and .075 for best efficiency and maximum pressure rise operation of the fan, respectively.

If the losses in the model are higher than in the test duct (as is more likely, due to the more complicated internal geometry) then the model exit area must be larger than that in the test rig to maintain the same mass flow since the peripheral jet total pressure is reduced. This has the effect of reducing J and the $h/\bar{c}$ ratio.

The two graphs indicate that operation of the fan in the model at its best efficiency point is desirable since this would produce the greater $h/\bar{c}$ ratio. Thus assuming that augmentation is independent of gap width, the exit area of the peripheral jet of the model should be adjusted so that the fan operates at its best efficiency point. If the assumptions of this analysis are valid and the losses in the model and test rig are not too dissimilar, $h/\bar{c}$ ratios of the order of .075 to .1 should be obtainable with the model. For the model's mean chord of about 6" this would correspond to hover heights of the order of .45" to .6".

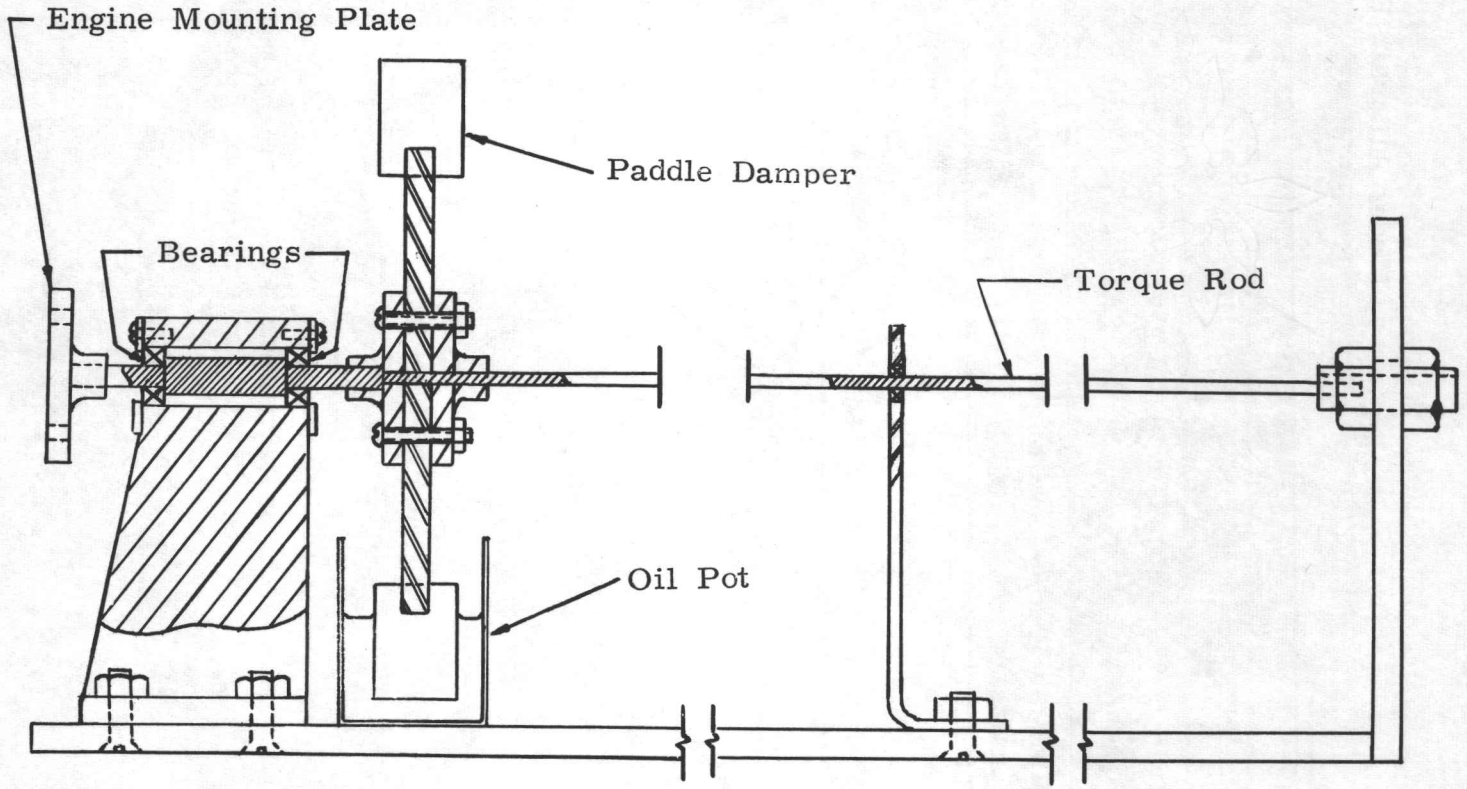

FIG. 1 MODEL ENGINE DYNAMOMETER

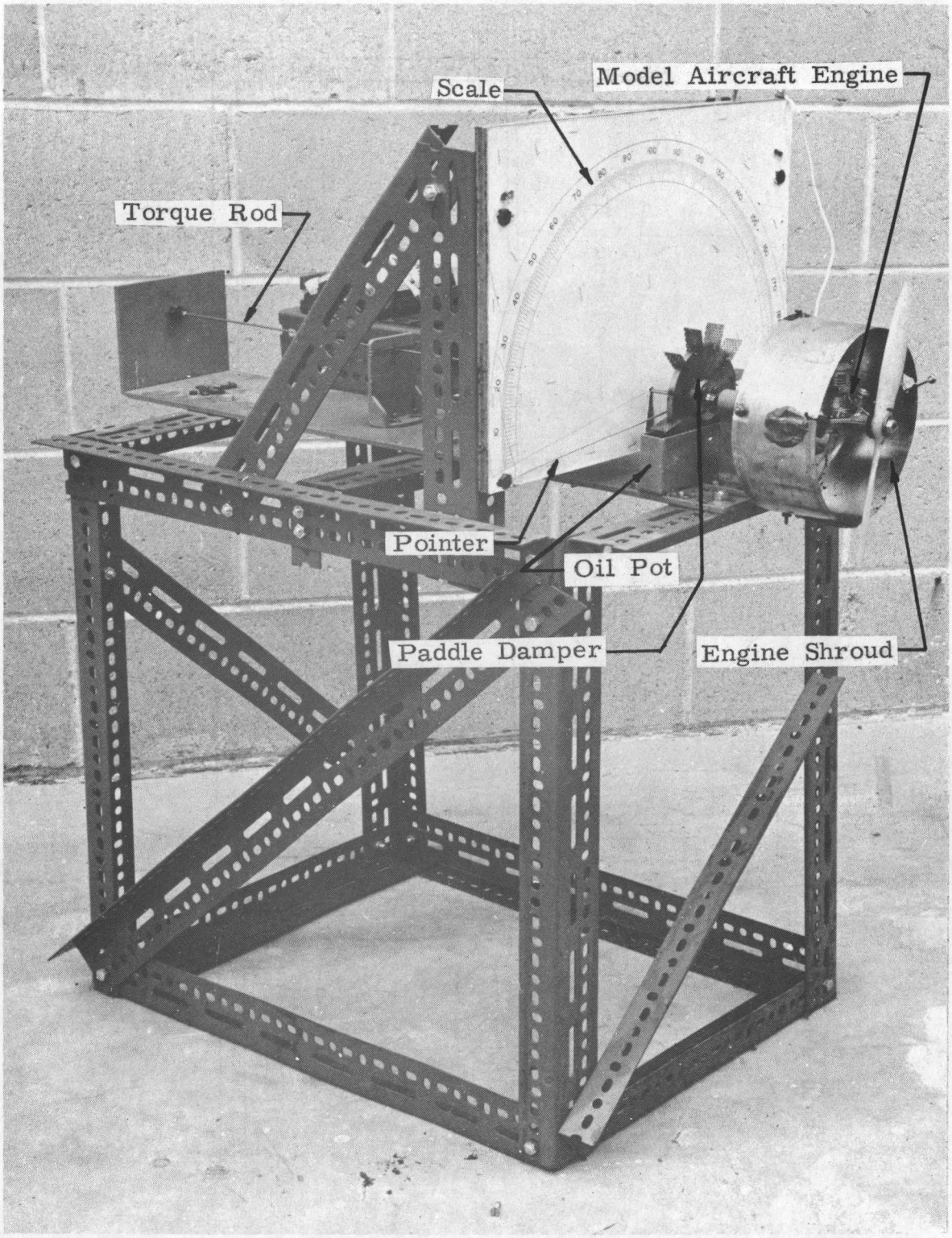

FIG. 2 MODEL ENGINE DYNAMOMETER

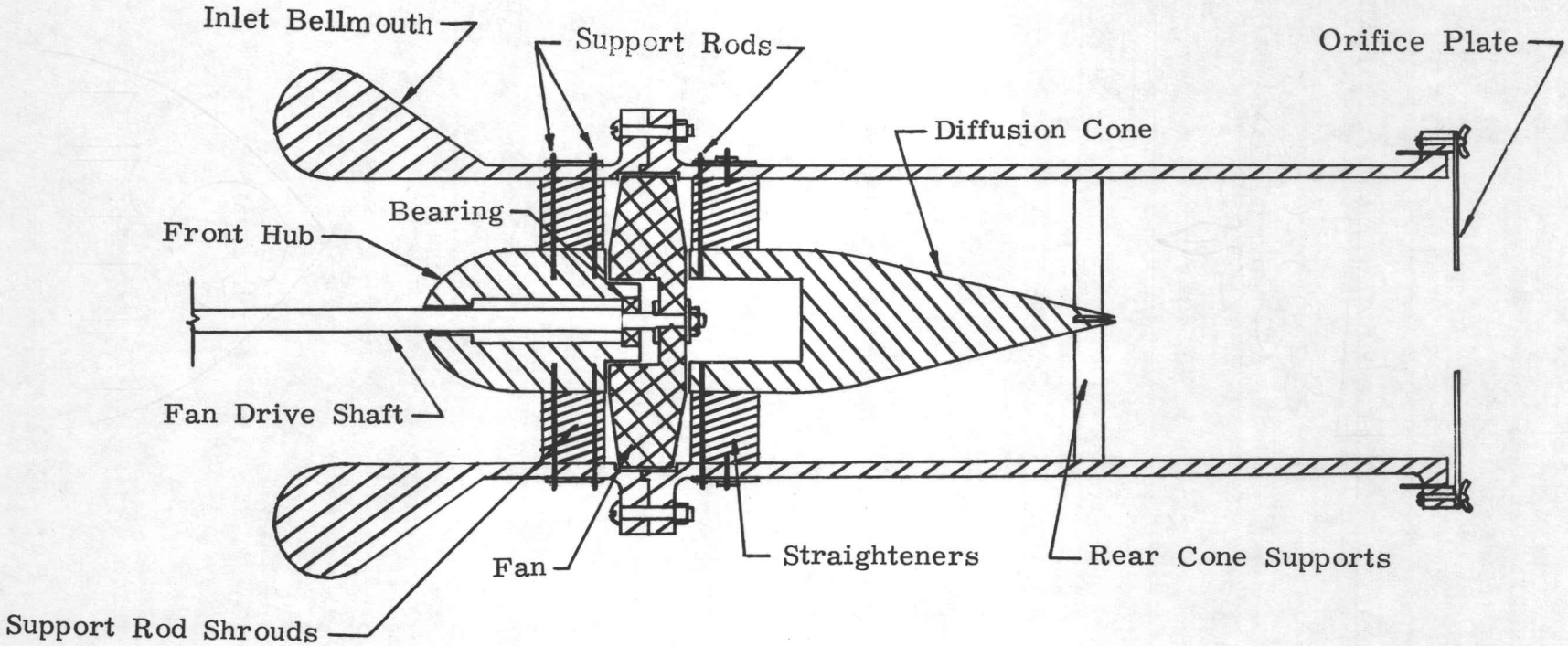

FIG. 3 FAN TEST RIG

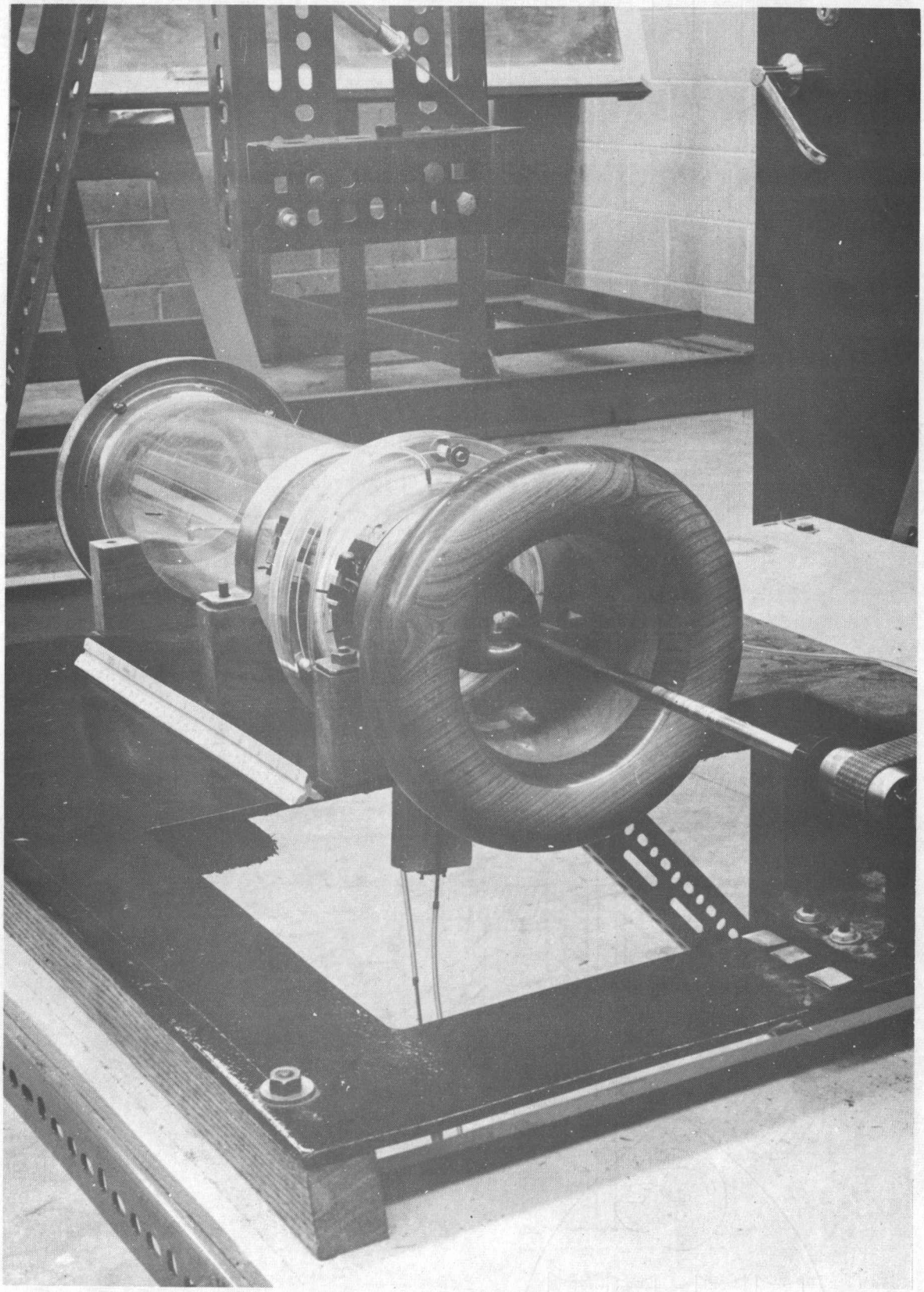

FIG. 4 FAN TEST RIG

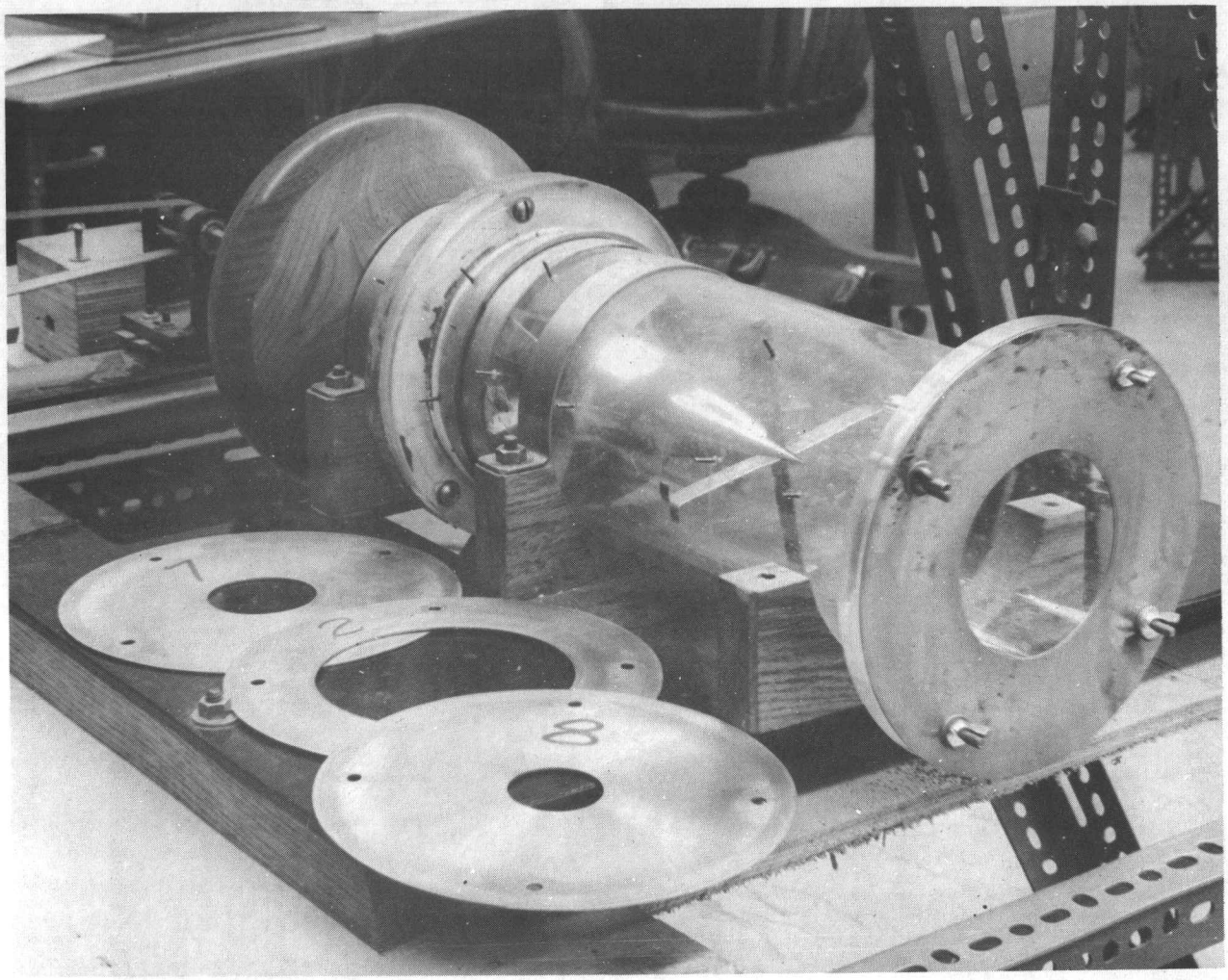

FIG. 5 REAR OF FAN TEST RIG SHOWING SEVERAL ORIFICE PLATES

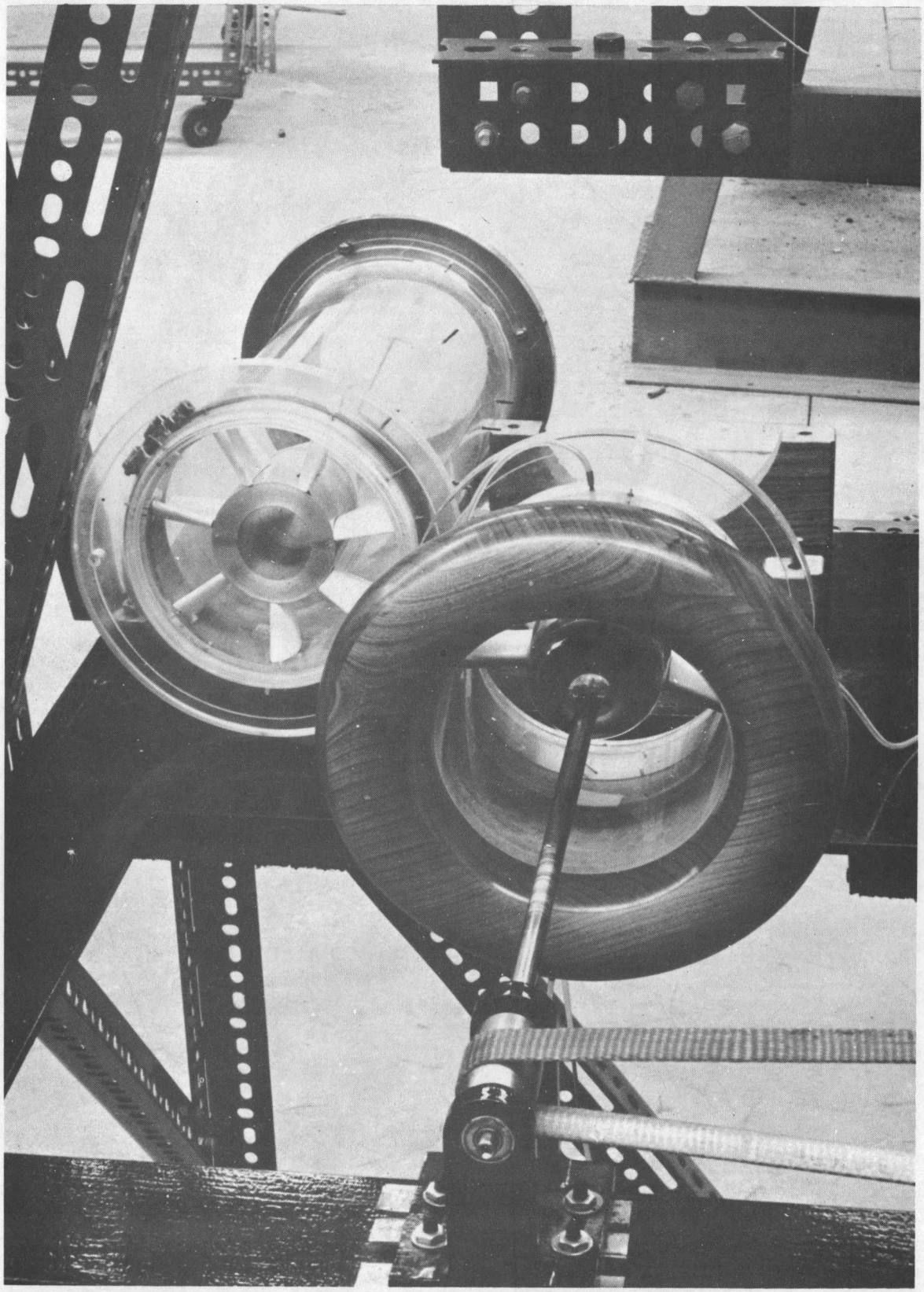

FIG. 6 TEST DUCT, SEPARATED, SHOWING

ADJUSTABLE STATORS IN REAR HALF

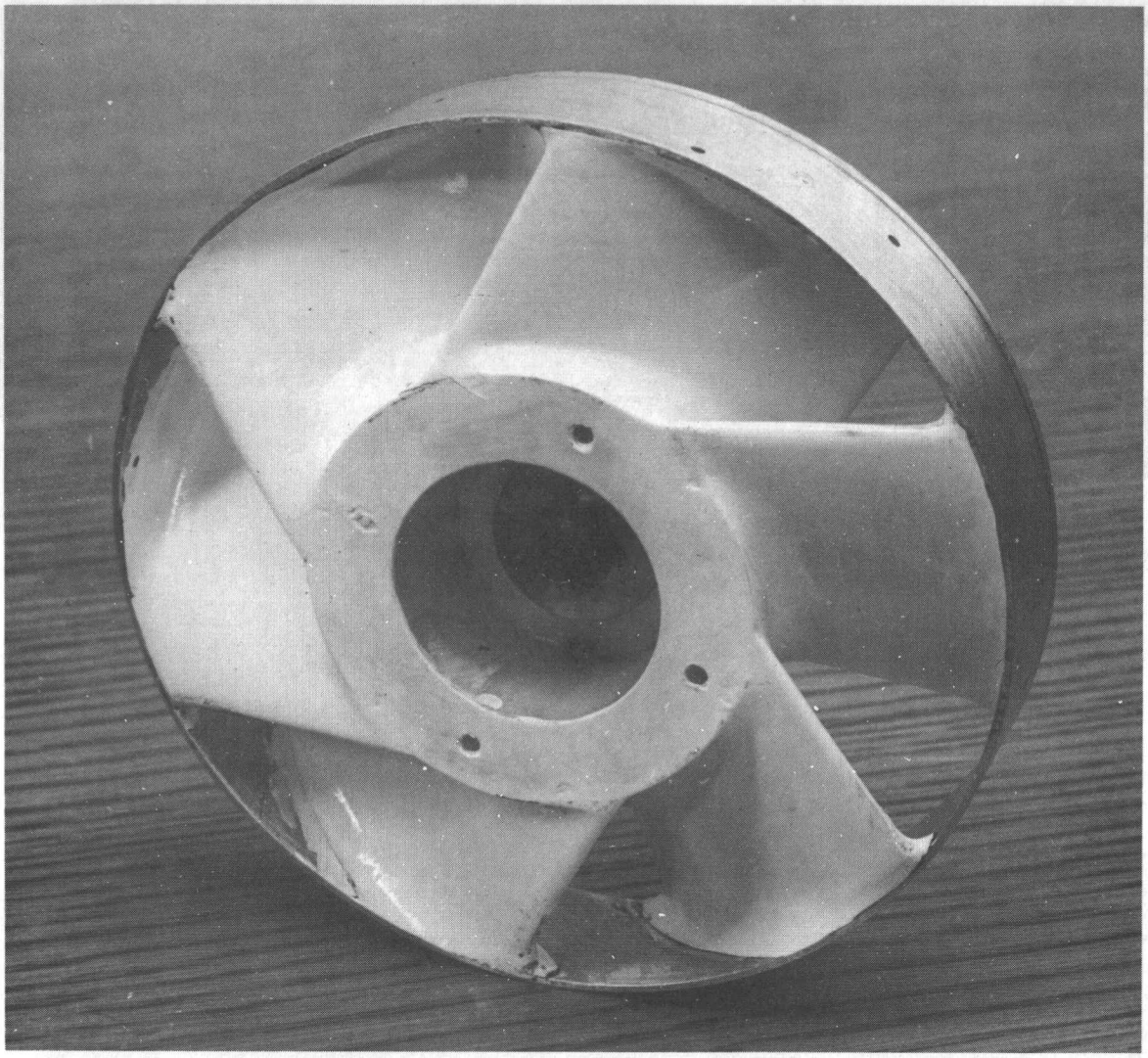

FIG. 7 FAN

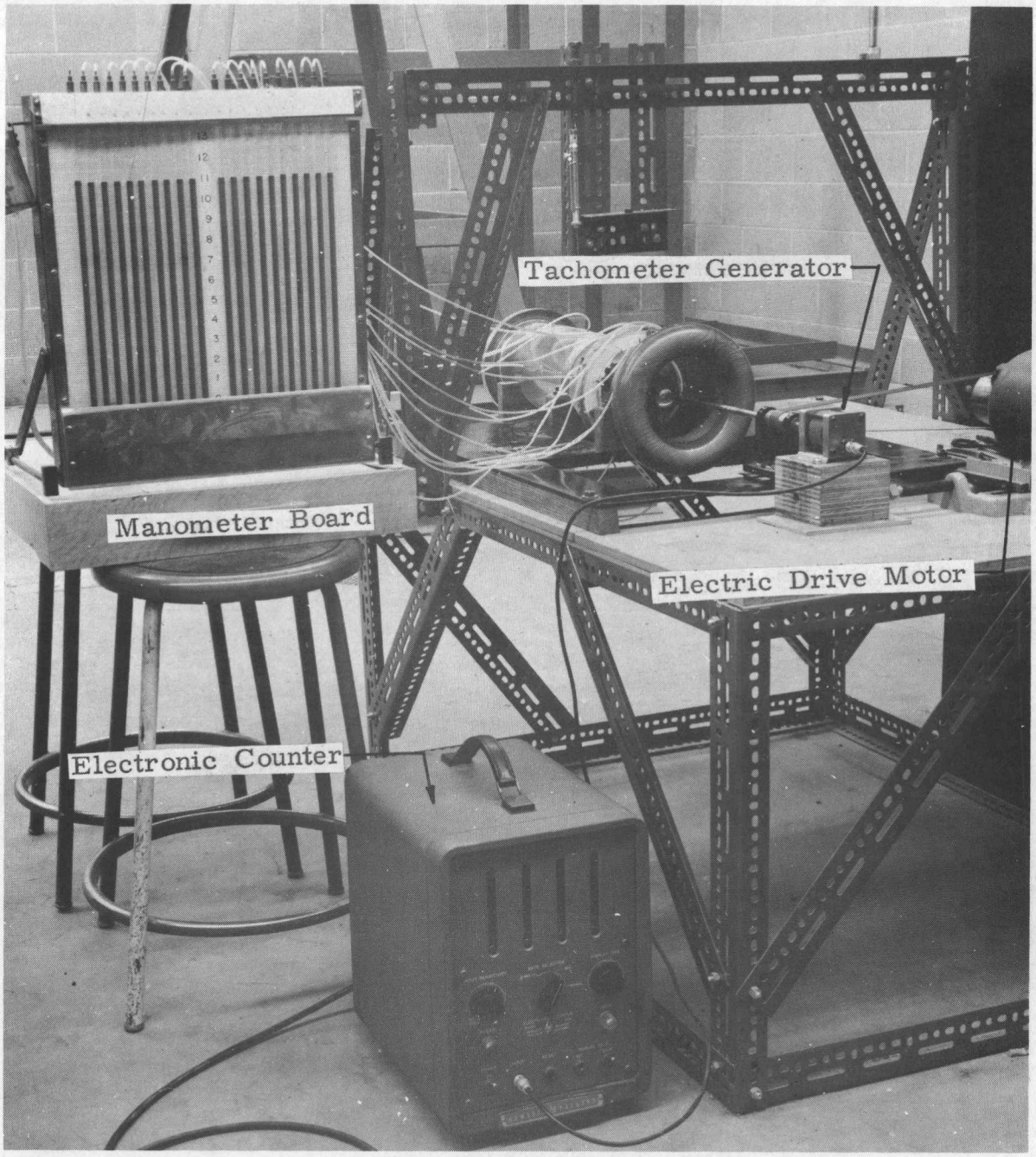

FIG. 8 FAN TEST RIG WITH ASSOCIATED INSTRUMENTATION

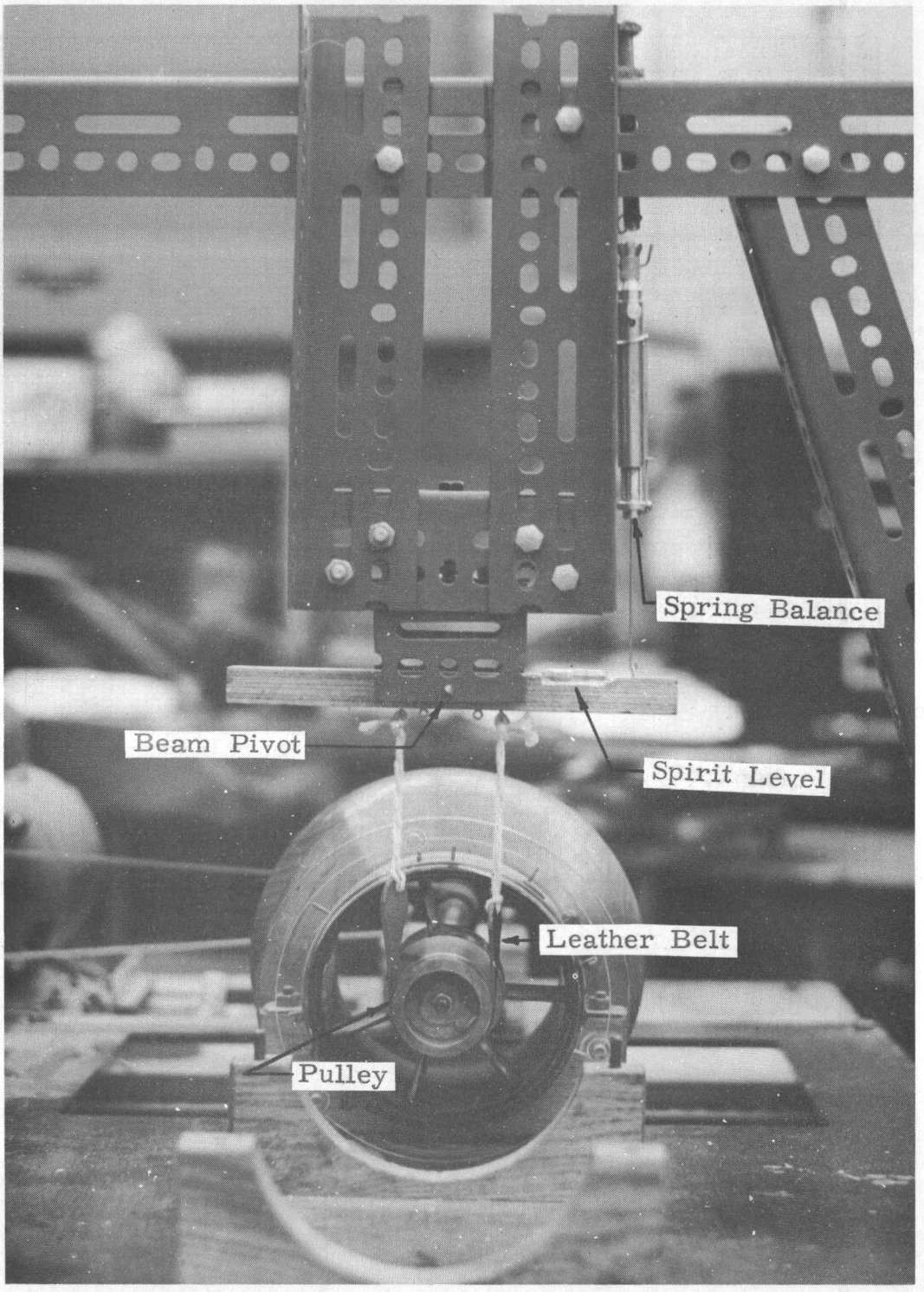

FIG. 9 PRONY BRAKE FOR CALIBRATION OF FAN DRIVE SHAFT

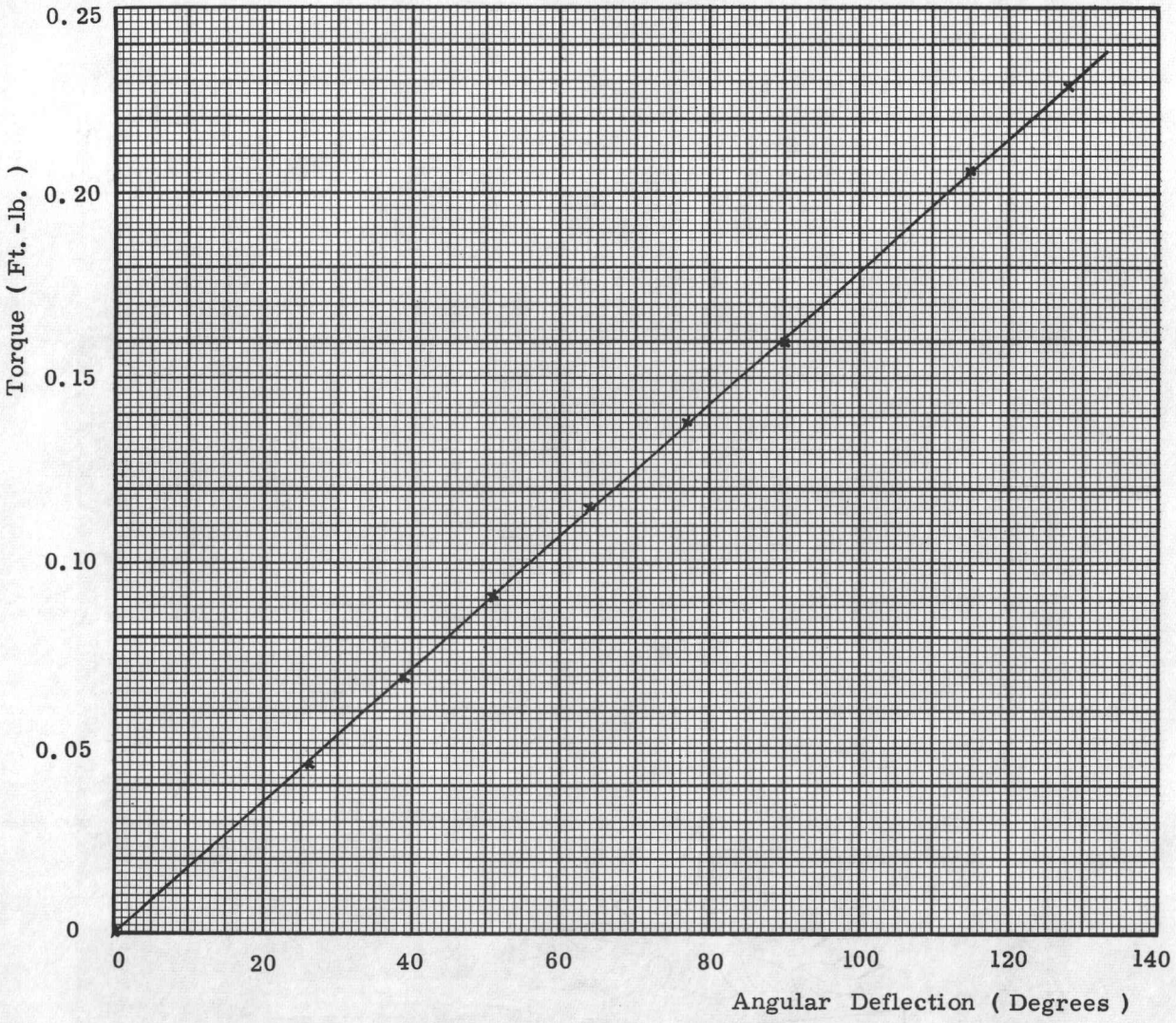

FIG. 10 CALIBRATION CURVE FOR 14 GAUGE TORQUE ROD

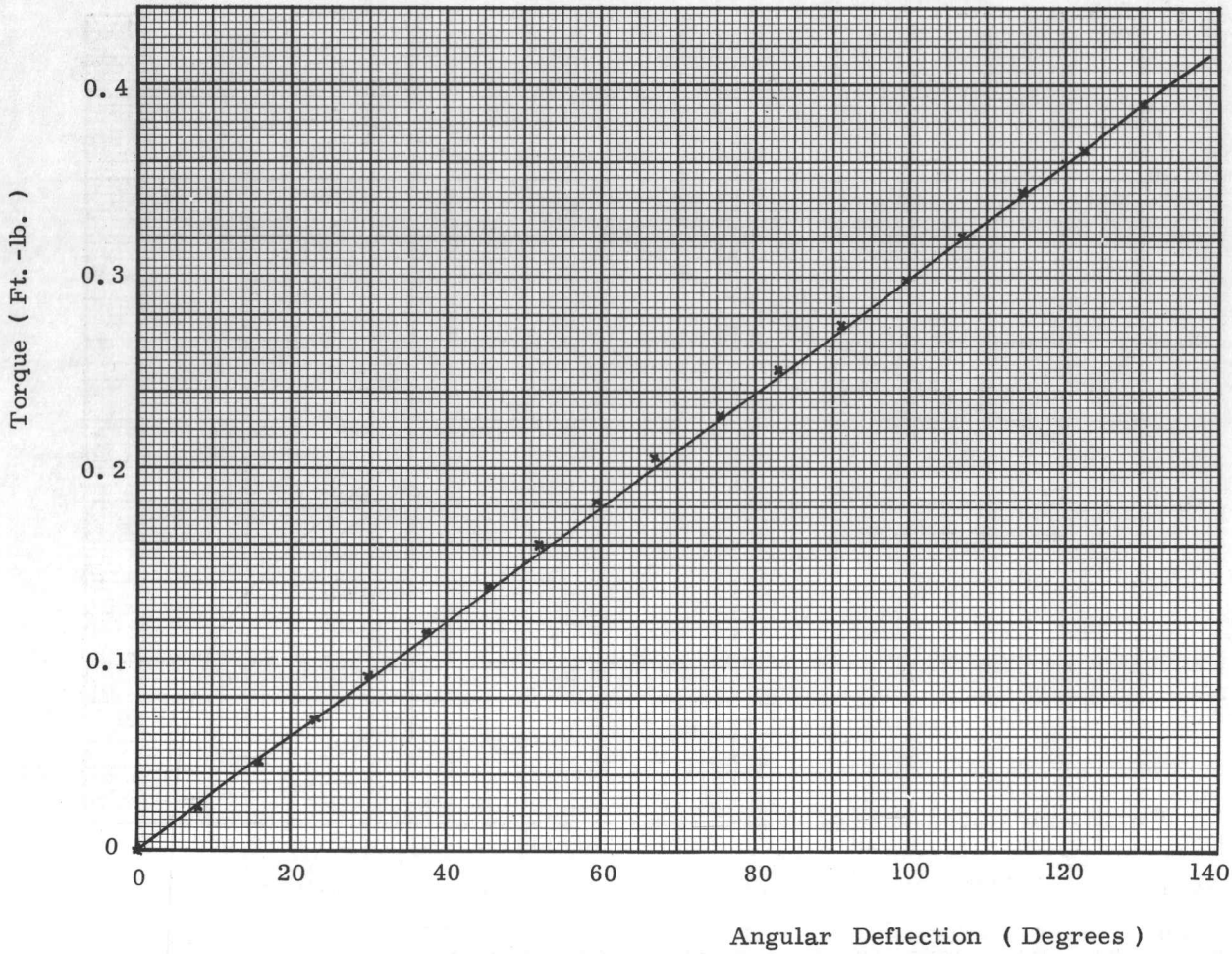

FIG. 11 CALIBRATION CURVE FOR 13 GAUGE TORQUE ROD

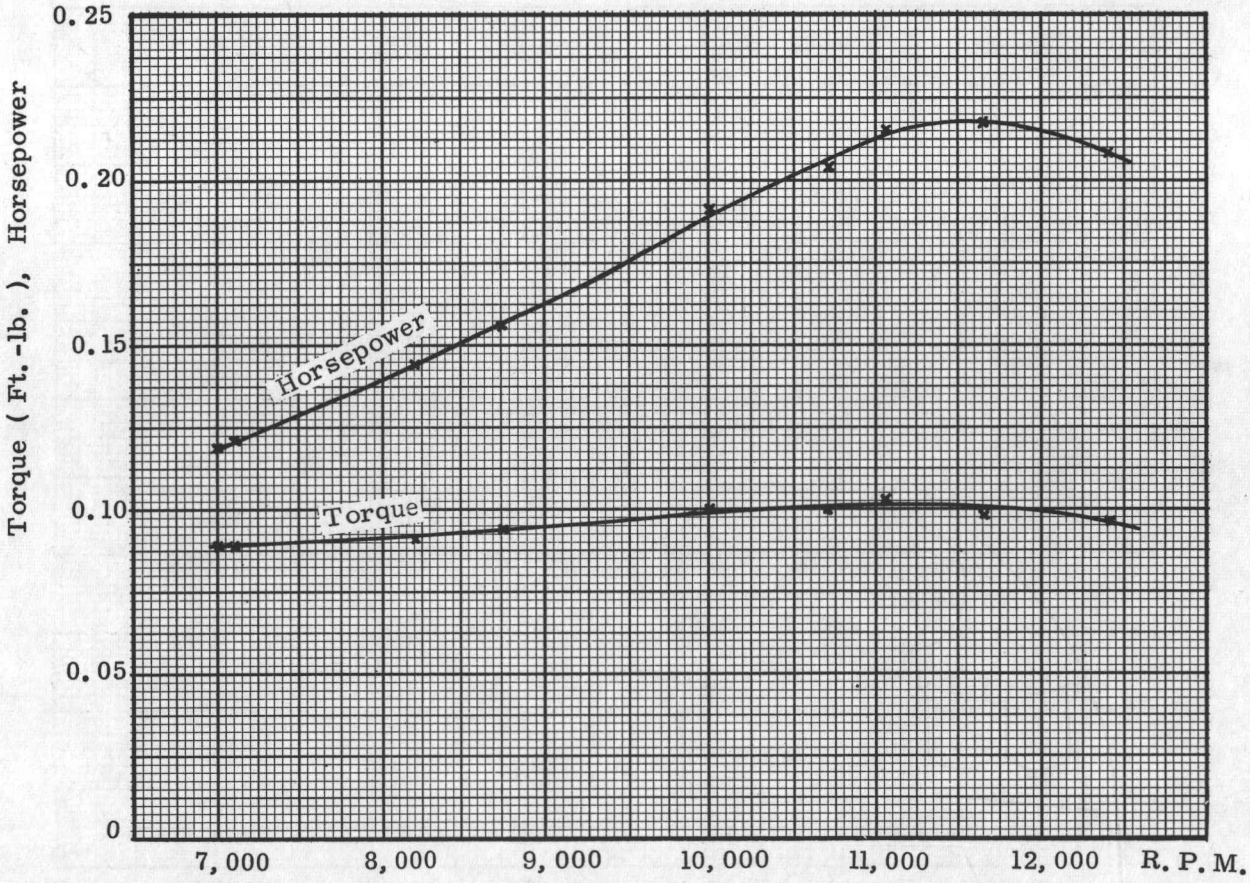

FIG. 12 TORQUE AND POWER OUTPUT OF .19 CU. IN. DISPLACEMENT ENGINE

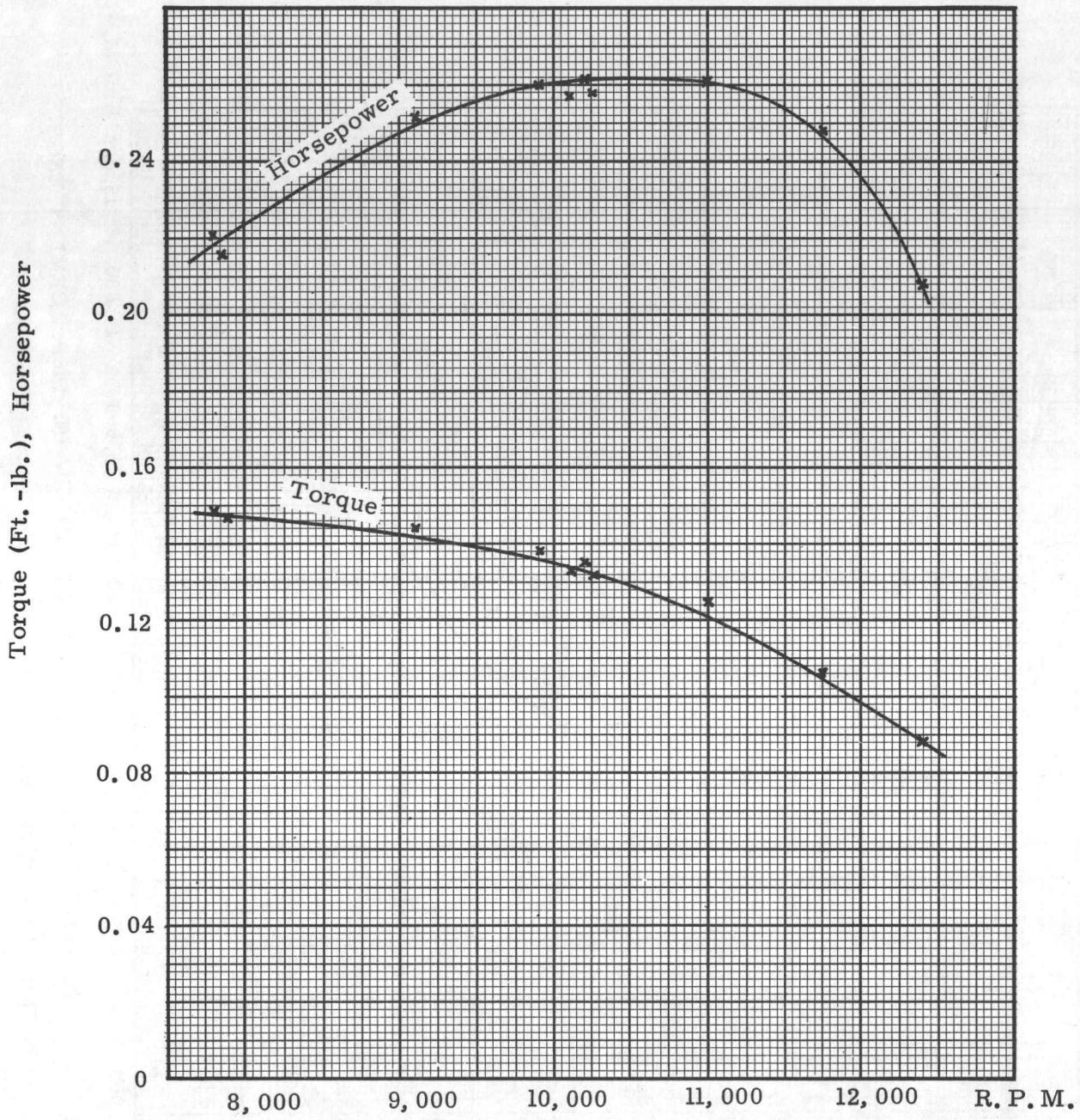

FIG. 13 TORQUE AND POWER OUTPUT OF .25 CU. IN. DISPLACEMENT ENGINE

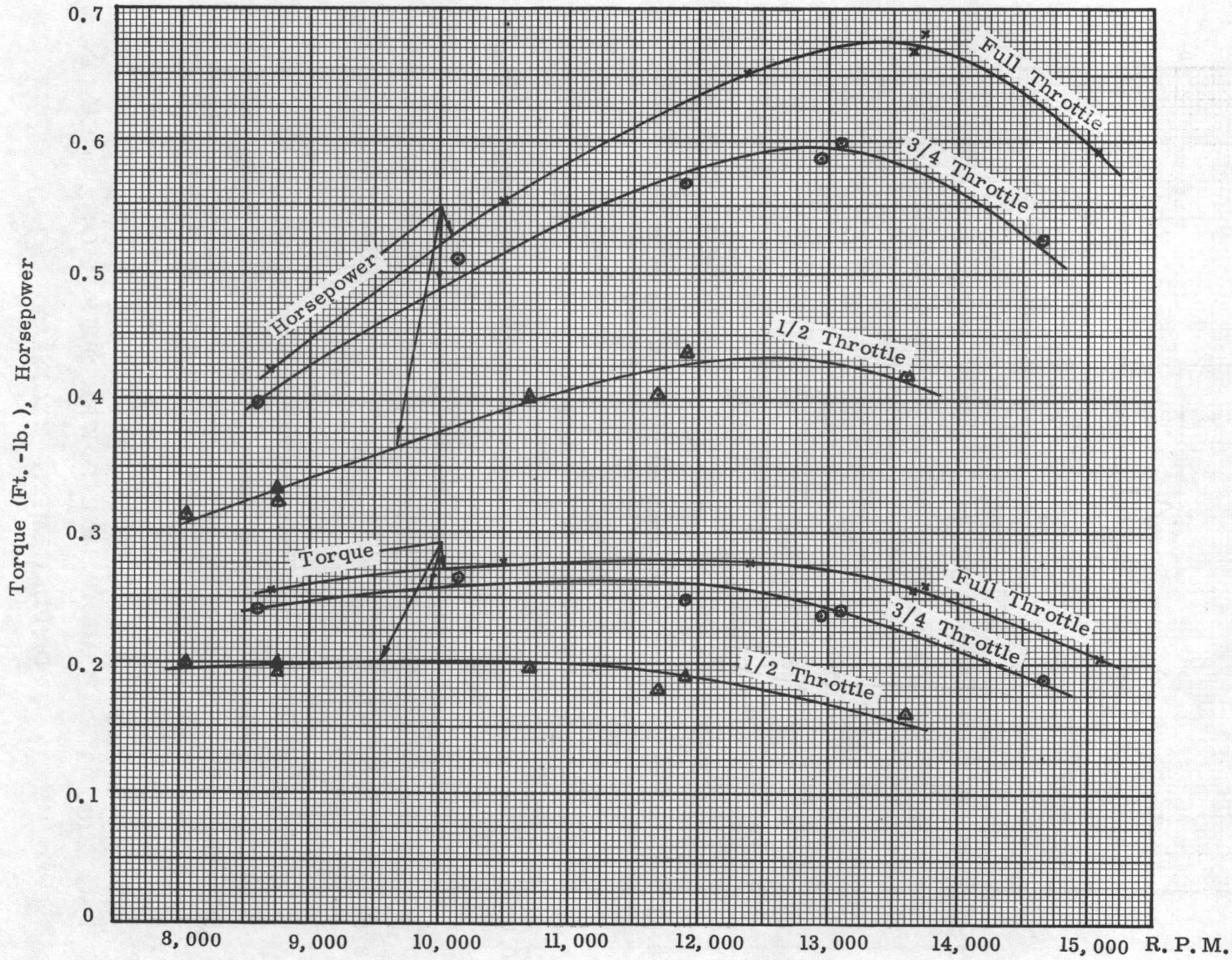

FIG. 14 TORQUE AND POWER OUTPUT FOR .35 CU. IN. DISPLACEMENT ENGINE FOR THREE THROTTLE SETTINGS

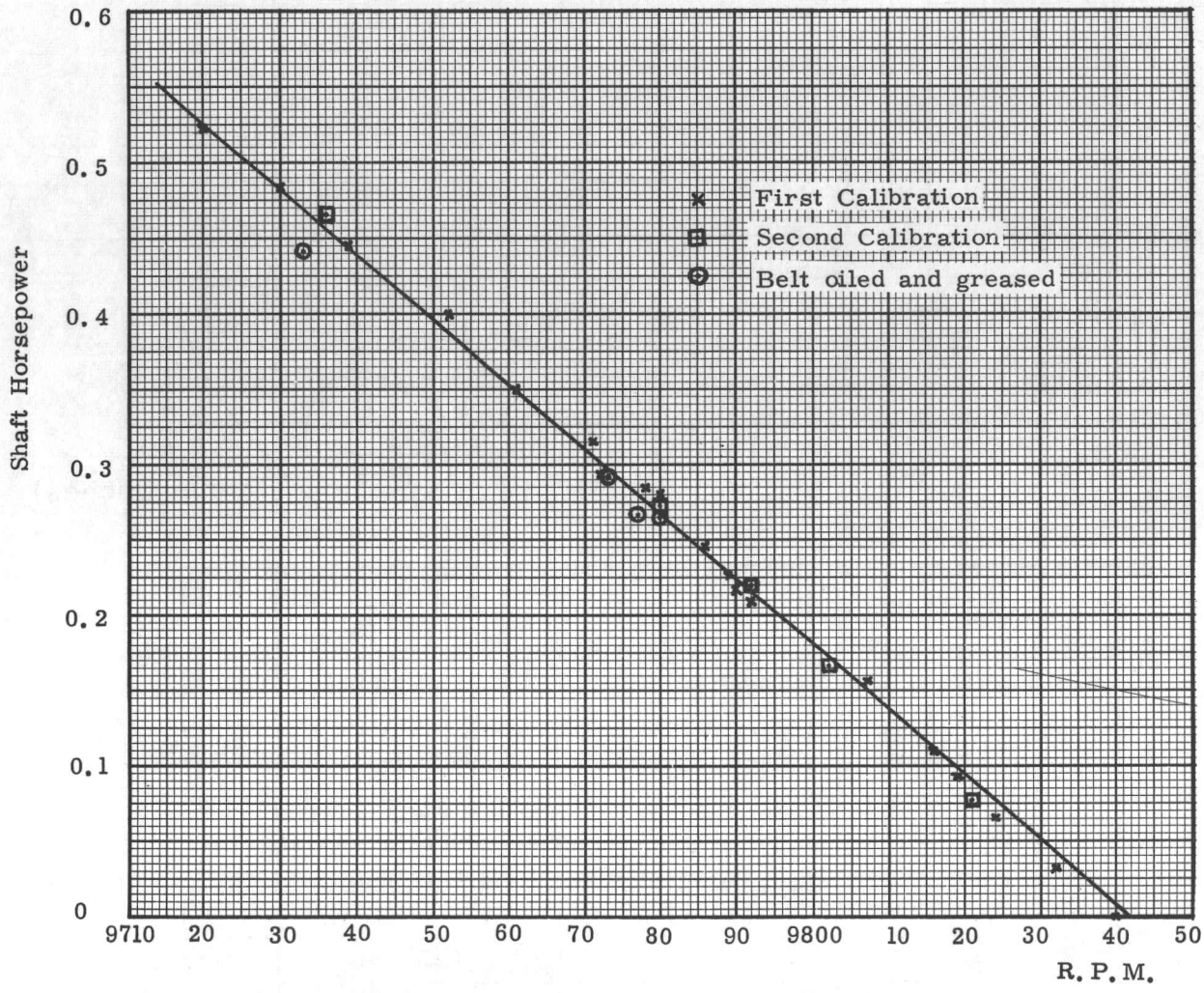

FIG. 15 CALIBRATION OF FAN DRIVE SHAFT

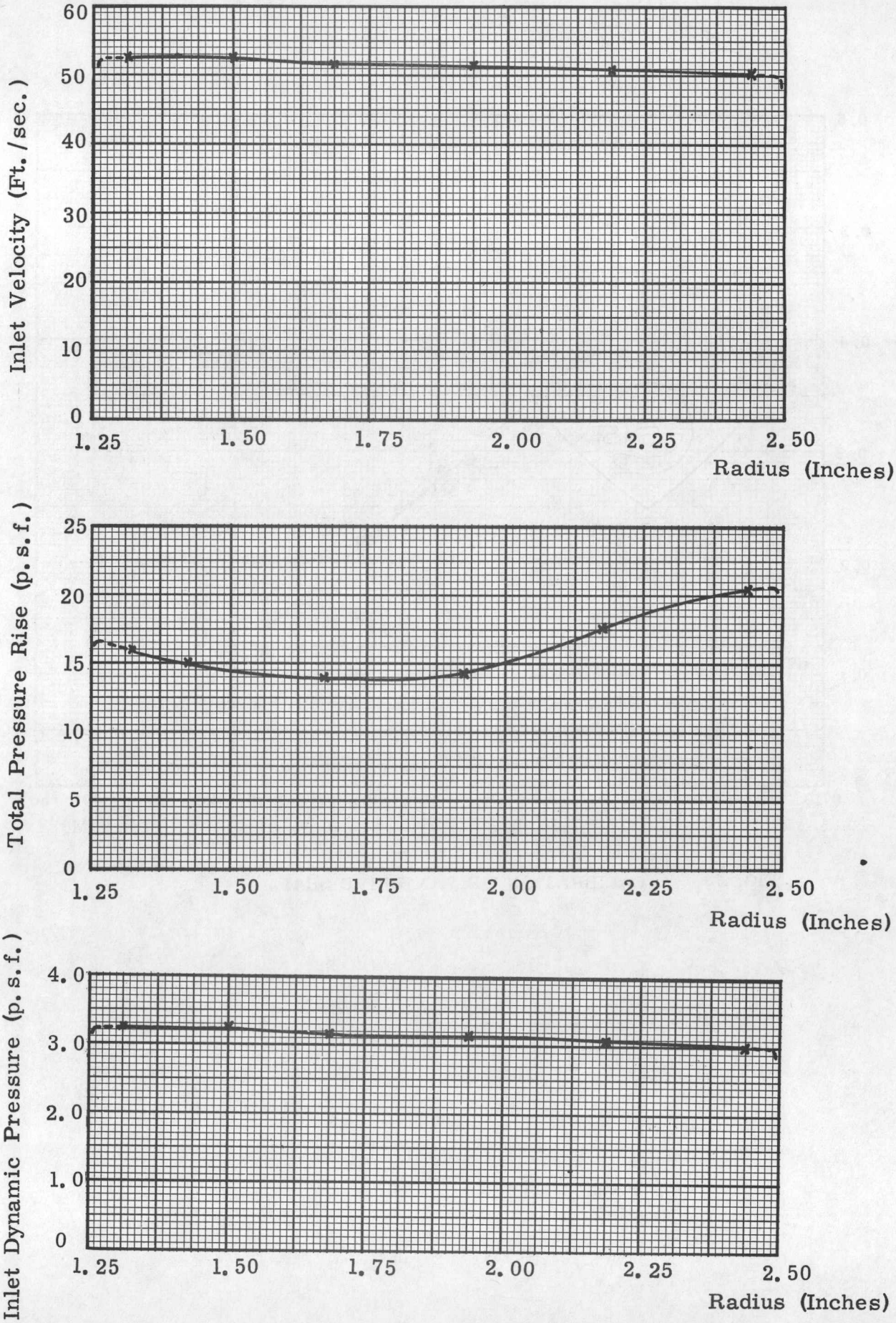

FIG. 16 PRESSURE AND VELOCITY DISTRIBUTIONS

($3\frac{1}{2}$" DIA. ORIFACE PLATE)

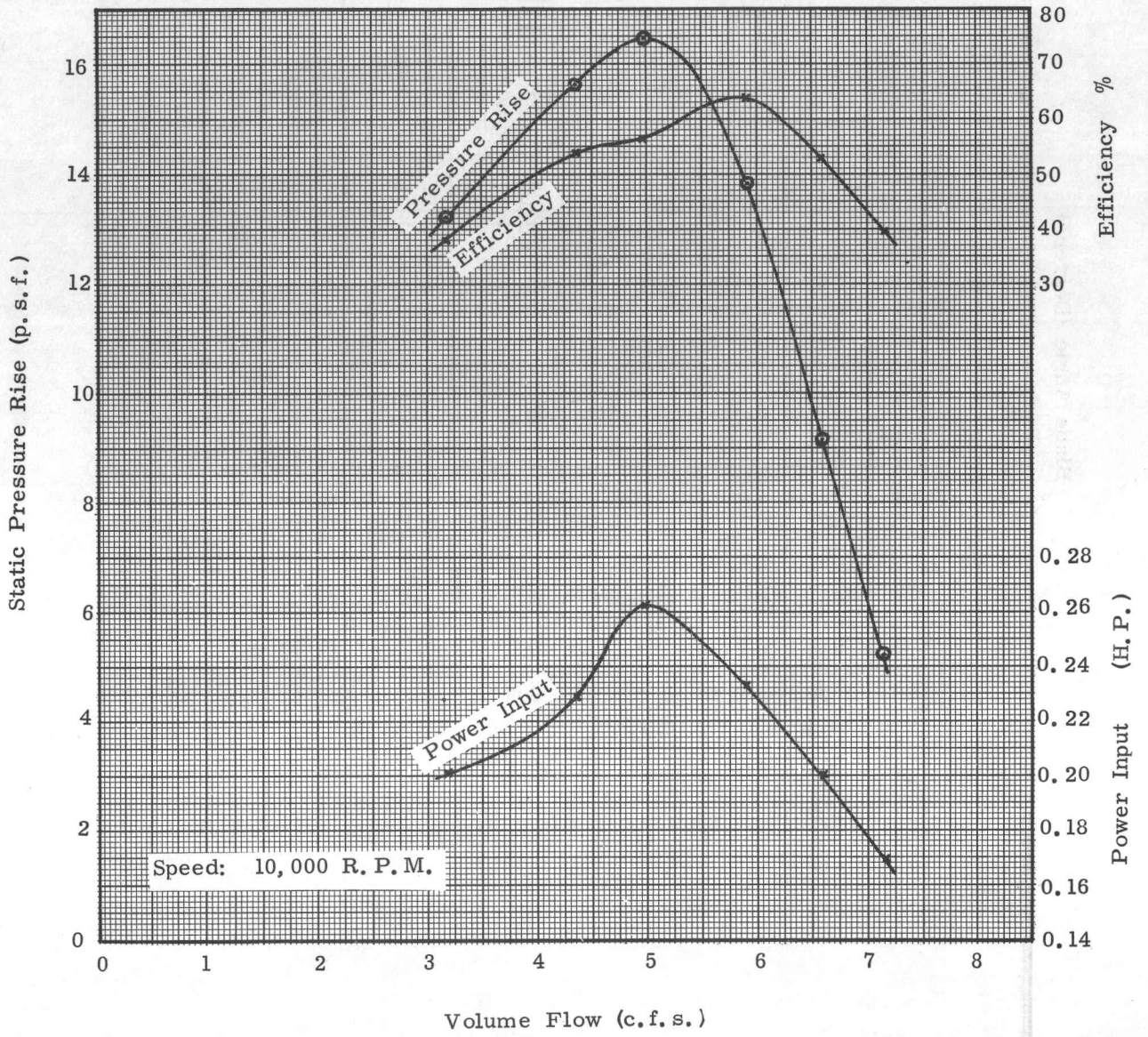

FIG. 17 FAN PERFORMANCE; PRESSURE RISE, POWER INPUT AND EFFICIENCY AS FUNCTIONS OF VOLUME FLOW AT CONSTANT SPEED

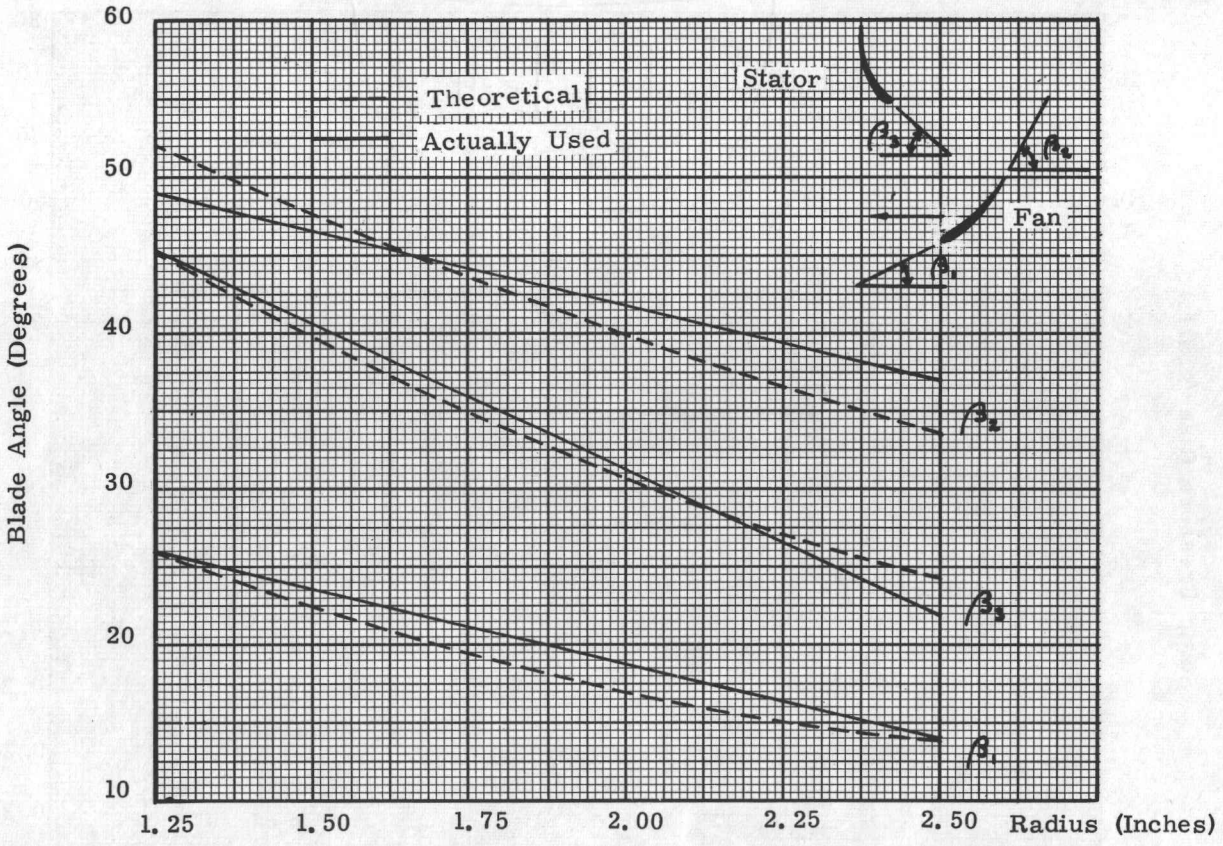

FIG. 18 THEORETICAL AND ACTUAL FAN BLADE ANGLES

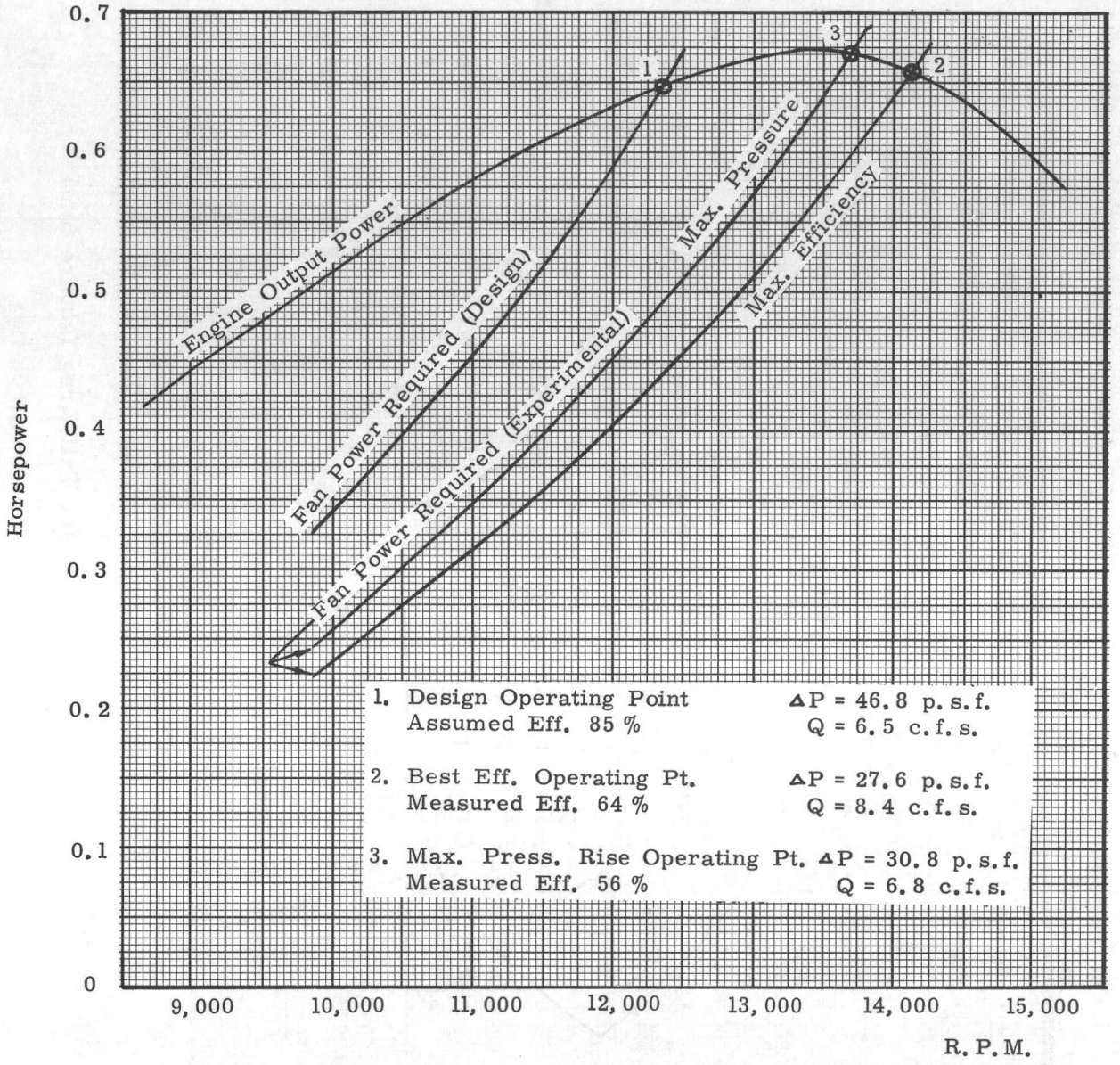

FIG. 19 FAN OPERATING POINTS, DESIGN AND EXPERIMENTAL

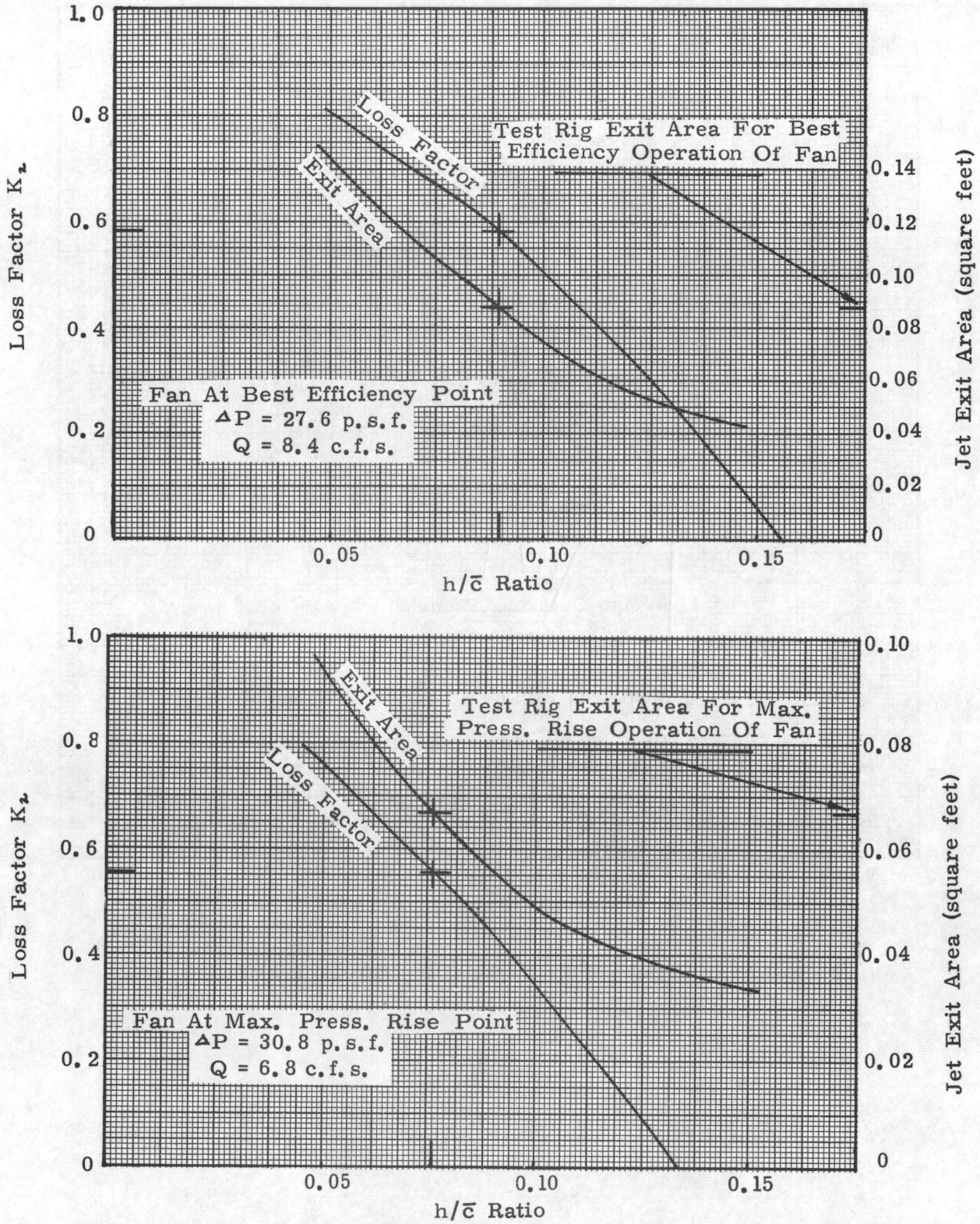

FIG. 20 JET EXIT AREA AND h/c̄ RATIO AS FUNCTIONS OF THE INTERNAL LOSSES